Electronic and Vibrational Close-Coupling Method for Resonant Electron-Molecule Scattering

Liam H. Scarlett⊙,* Igor Bray⊙, and Dmitry V. Fursa⊙

Curtin Institute for Computation and Department of Physics, Astronomy and Medical Radiation Sciences, Curtin University, Perth, Western Australia 6102, Australia

We report the development of a vibrational-electronic convergent close-coupling method for electron-molecule scattering with an *ab-initio* account of the coupling between the electronic and vibrational motions. The technique has been applied to scattering on molecular hydrogen, including coupling between vibrational levels in the first 11 electronic states. Distinct resonances associated with the temporary formation of the H_2^- ion are present between 10 and 14 eV for numerous transitions, including vibrational excitation of the $X\,^1\Sigma_g^+$ state, dissociation via the $b\,^3\Sigma_u^+$ state, and excitation of the $B\,^1\Sigma_u^+$ state. With both resonant and nonresonant scattering treated in a single calculation, this method is capable of providing self-consistent sets of cross sections for electron-molecule scattering in regions where the adiabatic-nuclei approximation breaks down.

Over the last few decades it has been the goal of the convergent close-coupling (CCC) method to provide a "complete scattering theory"—one capable of accurately describing all processes of interest over the entire range of collision energies for a given scattering system [1]. The *ab initio* CCC method is particularly well suited for this endeavor, since its expansion of the total scattering wave function over the target states explicitly couples all reaction channels, and the pseudostate representation of the target continuum allows accurate elastic, excitation, and ionization amplitudes to be extracted from a single calculation [2,3]. The distinguishing feature of CCC compared with other methods based on the close-coupling principle is the efficiency of its implementation, allowing large-scale convergence studies to be performed. For electron and positron scattering on quasi one- and two-electron targets, the CCC method can be considered a complete scattering theory.

The molecular CCC (MCCC) method is a separate implementation of the CCC theory for scattering on molecular targets, and has been shown to completely solve the electronic scattering problem for collisions with molecular hydrogen (H_2) within the fixed-nuclei (FN) approximation [4]. The extension of the MCCC method to generate vibrationally resolved cross sections using the adiabatic-nuclei (AN) approximation has been a major step forward in producing a comprehensive set of data for electron scattering on H_2 and its isotopologues [5,6]. However it is well known that the AN approximation is unable to describe resonant processes, even approximately. For electron-atom scattering, close-coupling methods are able to properly represent resonances in the calculated cross

sections by virtue of the implicit representation of the compound states in the close-coupling expansion of the scattering wave function. A similar implicit treatment of resonances in molecular scattering requires both electronic and nuclear states of the target to be included in the close-coupling expansion, leading to calculations which have historically been intractable. Current methods for the computation of resonant scattering cross sections typically utilize the projection-operator formalism of Feshbach [7] to project out the nonresonant scattering channels and explicitly couple the target and compound states involved in each transition [8–13]. These techniques require input from electronic scattering calculations (generally R matrix) for the resonance energies and widths, before solving the nuclear dynamics problem.

Our goal now is to incorporate resonant scattering into the MCCC method, with the motivation of having a single theoretical framework within which all scattering processes of interest can be calculated. As a first step, we continue to treat the rotational motion adiabatically, but explicitly couple the electronic and vibrational motions. We refer to this method as vibrational-electronic molecular convergent close-coupling (VE MCCC). For simplicity, we assume that the Born-Oppenheimer approximation is valid for the target states, allowing us to write the close-coupling expansion for the vibronic (vibrational and electronic) scattering state $|\Psi_{iv_i}^{(+)}\rangle$ as

$$|\Psi_{iv_i}^{(+)}\rangle \approx |\Psi_{iv_i}^{\mathcal{N}(+)}\rangle = \mathcal{A} \sum_{(n,v)\in\mathcal{N}} |f_{nv,iv_i}^{\mathcal{N}(+)}\rangle|\Phi_n\rangle|\nu_{nv}\rangle, \quad (1)$$

where $\mathcal{A}$ is the antisymmetrization operator, $|f_{nv,iv_i}^{\mathcal{N}(+)}\rangle$ are the multichannel projectile states, $|\Phi_n\rangle$ is an electronic target state, $|\nu_{nv}\rangle$ is a target vibrational state in the electronic state n, and $\mathcal{N}$ denotes the set of all vibronic states included in the expansion.

The corresponding momentum-space close-coupling equations for the scattering T matrix are

$$\langle \boldsymbol{q}_f \nu_{fv_f} \Phi_f | T | \Phi_i \nu_{iv_i} \boldsymbol{q}_i \rangle = \langle \boldsymbol{q}_f \nu_{fv_f} \Phi_f | V | \Phi_i \nu_{iv_i} \boldsymbol{q}_i \rangle + \sum_{(n,v)\in\mathcal{N}} \int \langle \boldsymbol{q}_f \nu_{fv_f} \Phi_f | V | \Phi_n \nu_{nv} \boldsymbol{q} \rangle G_{nv}^{(+)}(q) \langle \boldsymbol{q} \nu_{nv} \Phi_n | T | \Phi_i \nu_{iv_i} \boldsymbol{q}_i \rangle \mathrm{d}\boldsymbol{q}, \quad (2)$$

where T and V are the transition and interaction-potential operators, respectively, and $G_{nv}^{(+)}(q)$ is the asymptotic Green's function. The solution of the Lippmann-Schwinger equations [Eq. (2)] proceeds in a similar manner as in the FN MCCC method [14]. The representation of the vibronic scattering state in a complete basis [Eq. (1)] implicit in the solution of these equations leads to an accurate description of the compound three-electron states. Hence, without requiring explicit information about the resonance states, we expect to see the effects of both resonant and nonresonant scattering in the calculated cross sections. Further developments to include rearrangement channels explicitly, in a similar manner to the two-center CCC method for positron scattering on atoms [15], would allow cross sections for the important dissociative electron attachment process to be extracted.

The interaction potential contains both the direct and exchange interactions:

$$V = V_d + V_{\mathrm{exch}}, \quad (3)$$

the latter arising due to the antisymmetrization operator in Eq. (1). The Born-Oppenheimer representation of the target states allows for a simplification of the direct V-matrix elements by calculating the electronic matrix element first as a function of the internuclear separation before performing the vibrational integrations:

$$\langle \boldsymbol{q}' \nu_{n'v'} \Phi_{n'} | V_d | \Phi_n \nu_{nv} \boldsymbol{q} \rangle = \langle \nu_{n'v'} | \langle \boldsymbol{q}' \Phi_{n'} | V_d | \Phi_n \boldsymbol{q} \rangle | \nu_{nv} \rangle. \quad (4)$$

The electronic matrix elements are taken from the spheroidal-coordinate implementation of the MCCC method to ensure their accuracy at all internuclear separations required (see Ref. [16] for details of the spheroidal implementation). The exchange potential operator is given by

$$V_{\mathrm{exch}} = (E - H_{\mathrm{el}} - K_{\mathrm{vib}}) \sum_{j=1}^{2} P_{0j}, \quad (5)$$

where P_{0j} is the spin- and space-exchange operator, E is the total scattering energy, H_{el} is the electronic scattering-system Hamiltonian, and K_{vib} is the target vibrational kinetic-energy operator. We apply the common approximation of neglecting the effect of K_{vib} on the electronic target wave functions [17], which are assumed to vary slowly with R compared with the vibrational wave functions, so the exchange V-matrix element can be expressed as

$$\langle \boldsymbol{q}' \nu_{n'v'} \Phi_n | V_{\mathrm{exch}} | \Phi_n \nu_{nv} \boldsymbol{q} \rangle$$

$$= \langle \nu_{n'v'} | \langle \boldsymbol{q}' \Phi_{n'} | (E - H_{\mathrm{el}}) \sum_{j=1}^{2} P_{0j} | \Phi_n \boldsymbol{q} \rangle | \nu_{nv} \rangle$$

$$- \langle \nu_{n'v'} | \langle \boldsymbol{q}' \Phi_{n'} | \sum_{j=1}^{2} P_{0j} | \Phi_n \boldsymbol{q} \rangle K_{\mathrm{vib}} | \nu_{nv} \rangle. \quad (6)$$

In this Letter, we investigate resonances in the cross sections for scattering on the ground (electronic and vibrational) state of H_2, considering pure vibrational excitation, dissociation via the $b\,^3\Sigma_u^+$ state, and excitation of the $B\,^1\Sigma_u^+$ state, in the 10–14 eV energy region. The most prominent resonance in this region is the well-known $C\,^2\Sigma_g^+$ state of H_2^-, which has been the focus of many previous studies [12,13,18]. A number of resonances of other symmetries have also been identified by Stibbe and Tennyson [19]. We have performed VE MCCC calculations including the $X\,^1\Sigma_g^+$, $b\,^3\Sigma_u^+$, $a\,^3\Sigma_g^+$, $B\,^1\Sigma_u^+$, $c\,^3\Pi_u$, $EF\,^1\Sigma_g^+$, $C\,^1\Pi_u$, $e\,^3\Sigma_u^+$, $h\,^3\Sigma_g^+$, $B'\,^1\Sigma_u^+$, and $d\,^3\Pi_u$ electronic states of H_2, and a projectile partial-wave expansion with $L_{\mathrm{max}} = 6$. This model yields sufficiently converged cross sections (within 5%) for the transitions and incident energies of interest. Previous R-matrix studies have shown that an accurate representation of the H_2^- resonance states can be achieved using an expansion with fewer than ten low-lying H_2 states [19,20], so we expect the present model to give an accurate account of resonant scattering.

The close-coupling expansion [Eq. (1)] includes bound vibrational states as well as vibrational pseudostates which discretize the dissociative continuum of each electronic state, leading to an account of dissociation equivalent to the pseudostate treatment of ionization in the CCC or R matrix with pseudostate methods [21,22]. Convergence in the transitions of interest was confirmed with respect to the number of vibrational levels included, with the final calculations containing a total of 587 vibronic states. To handle the large number of coupled equations in
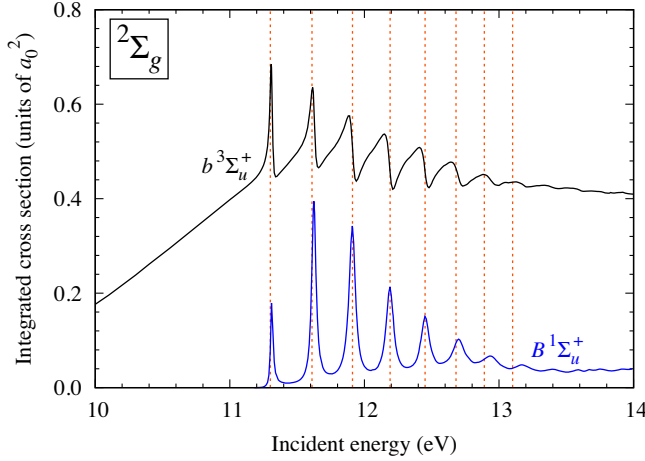
FIG. 1. Electron-impact cross sections for excitation of the $b\,^3\Sigma_u^+$ and $B\,^1\Sigma_u^+$ states of H_2 from the ground state, considering only the $^2\Sigma_g$ scattering symmetry. The vertical dashed lines indicate the $C\,^2\Sigma_g^+$ vibrational energy levels of the H_2^- ion determined experimentally by Comer and Read [23].

FIG. 2. Illustration of the resonant and nonresonant processes contributing to the $X\,^1\Sigma_g^+ \to b\,^3\Sigma_u^+$ transition. The H_2 potential-energy curves are taken from Refs. [26–28], and the H_2^- curve from Ref. [19]. The vibrational energies of the $C\,^2\Sigma_g^+$ state are taken from Ref. [23].

Eq. (2) we utilize a hybrid OpenMP-MPI parallelism scheme with the V matrix distributed across many supercomputer nodes.

In Fig. 1, we present the cross sections for excitation of the $b\,^3\Sigma_u^+$ and $B\,^1\Sigma_u^+$ states considering only the $^2\Sigma_g$ scattering symmetry. There are prominent resonances in both cross sections, associated with the temporary formation of the excited Rydberg $C\,^2\Sigma_g^+$ state of the H_2^- ion. The resonance positions are in excellent agreement with the experimentally determined vibrational energies of Comer and Read [23] for this state, which are indicated by the vertical dashed lines in the figure. Similar resonances were found in recent local complex-potential (LCP) calculations [13] of the D_2 $b\,^3\Sigma_u^+$ excitation, although these calculations do not include the nonresonant contribution.

An illustration of the resonant and nonresonant processes contributing to dissociation through the $b\,^3\Sigma_u^+$ state in the $^2\Sigma_g$ symmetry is provided in Fig. 2. The nonresonant process corresponds to the electronically free scattering channels, while the resonant process corresponds to the electronically bound scattering channels [24,25]. The resonant process proceeds via capture of the incident electron to form the H_2^- ion in one of a number of possible vibrational levels, before the compound state decays back into neutral H_2 plus a free electron. For a given final energy in the $b\,^3\Sigma_u^+$ continuum, the nonresonant process has a lower threshold than the resonant process because it does not require the formation of a higher-energy intermediate state. Each of the resonance peaks in the calculated cross section corresponds to the formation of a different vibrational level in the compound $C\,^2\Sigma_g^+$ state. The $C\,^2\Sigma_g^+$ state primarily decays into the $X\,^1\Sigma_g^+$, $b\,^3\Sigma_u^+$, and $B\,^1\Sigma_u^+$ states of H_2 [19], leading to similar resonance structures in the excitation cross sections for each of these states.
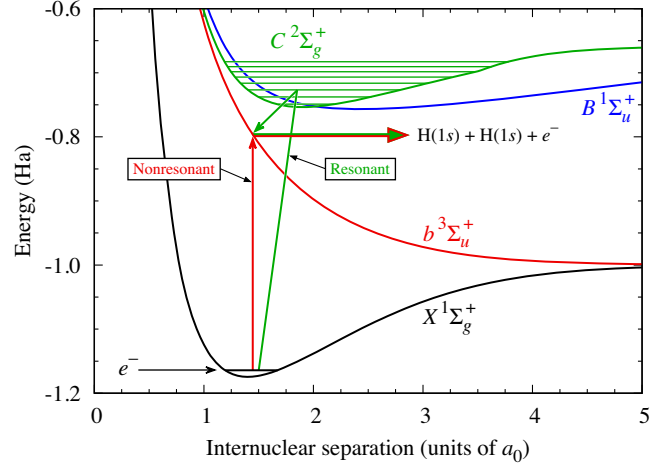
In Fig. 3 we present cross sections for excitation of the $b\,^3\Sigma_u^+$, $B\,^1\Sigma_u^+$, and $X\,^1\Sigma_g^+$ states, showing the contributions from the four dominant scattering symmetries: $^2\Sigma_u$, $^2\Sigma_g$, $^2\Pi_g$, and $^2\Pi_u$. The $B\,^1\Sigma_u^+$ cross section is summed over all final vibrational levels, while the $X\,^1\Sigma_g^+$ cross section is summed over levels $v_f > 0$ since the vibrationally elastic cross section is dominated by nonresonant scattering and would obscure the resonance structures. For dissociative excitation of the $b\,^3\Sigma_u^+$ state there are prominent resonances in both the $^2\Sigma_g$ and $^2\Pi_u$ symmetries, and barely visible features in the others. The $B\,^1\Sigma_u^+$ cross section has resonance structures in all four symmetries, which we compare with measured or calculated resonance positions taken from the literature: $^2\Sigma_g$ and $^2\Sigma_u$ from the measurements of Comer and Read [23], $^2\Pi_u$ from the calculations of Stibbe and Tennyson [19], and $^2\Pi_g$ from the measurements of Kuyatt et al. [29]. In the $^2\Sigma_u$ symmetry the present calculations appear to show a number of resonance features above the levels identified in Ref. [23]; however, inspection of the contributions from each exit vibrational level suggests these are the result of interference between nonresonant channels as higher vibrational levels open with increasing energy. In the $^2\Pi_g$ symmetry we do not see the first two resonances found by Kuyatt et al. [29], either because they were incorrectly identified, or because the calculated cross section is too small near the threshold for the resonances to be visible. In the $X\,^1\Sigma_g^+$ cross sections there are prominent peaks in the $^2\Sigma_g$ and $^2\Pi_u$ symmetries, with only faint features in the other two symmetries.

In Fig. 4 we present cross sections for pure vibrational excitations (from $v_i = 0$) within the $X\,^1\Sigma_g^+$ state in the $^2\Sigma_g$ scattering symmetry. The vibrationally elastic $v = 0 \to 0$

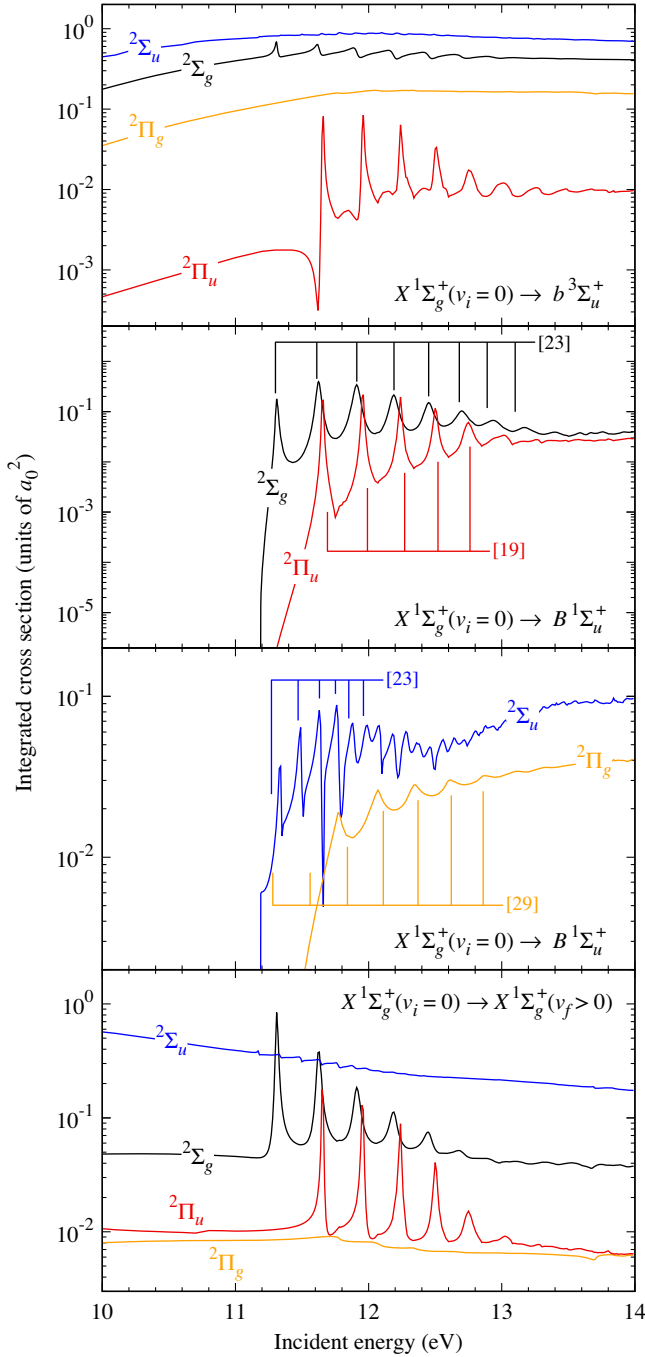FIG. 3. Electron-impact cross sections for excitation of the $b\,^3\Sigma_u^+$, $B\,^1\Sigma_u^+$, and $X\,^1\Sigma_g^+$ states of H$_2$ from the $X\,^1\Sigma_g^+(v_i = 0)$ state. The results are displayed separately for each of the four dominant scattering symmetries: $^2\Sigma_u$, $^2\Sigma_g$, $^2\Pi_u$, and $^2\Pi_g$. The $B\,^1\Sigma_u^+$ cross section is summed over the final vibrational levels, while the $X\,^1\Sigma_g^+$ cross section is summed over levels $v_f > 0$.

FIG. 4. Electron-impact cross sections in the $^2\Sigma_g$ scattering symmetry for excitation of the $v_f = 0 \to 14$ vibrational levels from the $v_i = 0$ level in the $X\,^1\Sigma_g^+$ state of H$_2$. Note the different vertical scale for the $v = 0 \to 0$ cross section.

cross section is dominated by nonresonant scattering. The nonresonant contribution diminishes with an increasing exit vibrational level, so that for $v_f > 2$ only the resonance peaks are visible. Celiberto *et al.* [12] have previously calculated cross sections for resonant vibrational excitation
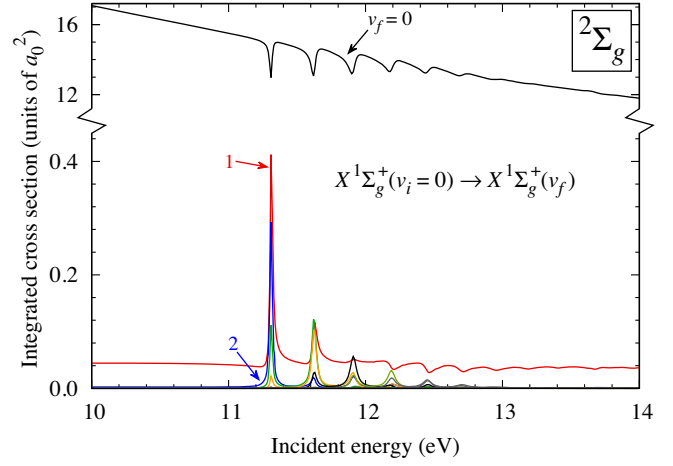
of H$_2$ involving the $^2\Sigma_g$ symmetry in this energy range, using the LCP method. Although the resonance structures seen in the LCP results are similar to those in the present calculations, the two data sets are not directly comparable, since the LCP calculations do not account for nonresonant scattering. In fact, the vibrationally elastic $v = 0 \to 0$ cross section presented by Celiberto *et al.* [12] has prominent resonance peaks corresponding to the $C\,^2\Sigma_g^+$ vibrational-level energies, while in the present calculations there are dips at the resonance energies in this cross section. A novel feature of our method which is not present in alternative approaches is the proper account of coupling between resonant and nonresonant scattering channels, which captures the redistribution of flux from nonresonant elastic scattering into the resonant excitations and leads to the dips in the $v = 0 \to 0$ cross section.

Resonances also appear in FN calculations of electron-molecule cross sections, associated with the formation of a compound state at the fixed internuclear separation. In Fig. 5 we compare the $X\,^1\Sigma_g^+(v_i = 0) \to b\,^3\Sigma_u^+$ cross section in the $^2\Sigma_g$ symmetry obtained using the present VE MCCC method with results obtained using the FN approximation. The FN calculation utilizes an electronic close-coupling expansion consisting of the same electronic states included in the VE MCCC calculations. Above 13 eV the two methods produce similar results, but in the resonance region the FN approximation clearly break down. The FN cross section has a prominent resonance just below 12 eV, corresponding to the vertical excitation energy of the H$_2^-$ $C\,^2\Sigma_g^+$ state at the mean internuclear separation [19]. Evidently, the FN approximation is able to roughly identify the energy region where the resonances should occur, but cannot predict the number of resonances or their positions. The magnitude of the FN resonance peak is also substantially larger than any of the true resonances.
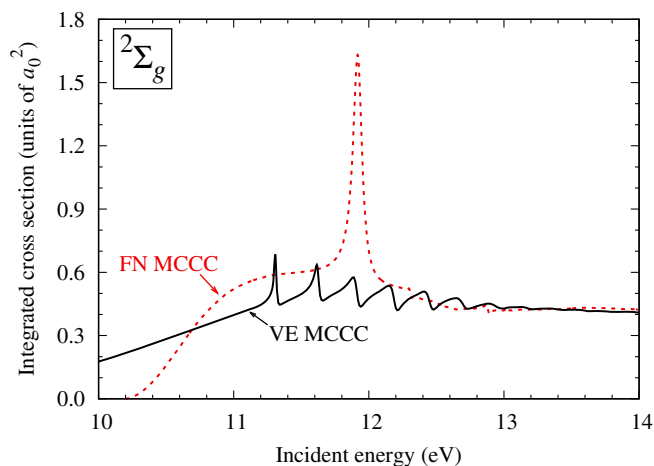
FIG. 5. Electron-impact cross sections in the $^2\Sigma_g$ scattering symmetry for excitation of the $b\,^3\Sigma_u^+$ state from the ground state of H_2. Comparison is between calculations performed with the vibrational-electronic and fixed-nuclei MCCC methods (VE MCCC and FN MCCC, respectively).

In this Letter we have demonstrated the feasibility of extending the MCCC method to include both electronic and nuclear states in the close-coupling expansion, allowing the calculation of self-consistent sets of absolute cross sections where the adiabatic-nuclei approximation breaks down. The method treats both resonant and nonresonant scattering on the same footing, and does not require the input of resonance data from external calculations. We have applied the method to the resonance structures in the 10–14 eV incident-energy region of electron scattering on H_2, and found agreement with previously measured or calculated resonance positions. As the MCCC method is extended to more complex diatomic molecules in the future, the techniques described here can be immediately applied. This will allow the benefits of large-scale close-coupling calculations, such as rigorous demonstrations of convergence and a proper account of interchannel coupling, to be applied to all molecular scattering processes. Thus, a complete description of electron-molecule scattering previously believed to be unfeasible is becoming within reach of present-day computational methods.

*liam.scarlett@postgrad.curtin.edu.au

[1] I. Bray and D. V. Fursa, Phys. Rev. Lett. **76**, 2674 (1996).
[2] X. Ren, I. Bray, D. V. Fursa, J. Colgan, M. S. Pindzola, T. Pflüger, A. Senftleben, S. Xu, A. Dorn, and J. Ullrich, Phys. Rev. A **83**, 052711 (2011).
[3] I. Bray, D. V. Fursa, A. S. Kadyrov, A. T. Stelbovics, A. S. Kheifets, and A. M. Mukhamedzhanov, Phys. Rep. **520**, 135 (2012).
[4] M. C. Zammit, J. S. Savage, D. V. Fursa, and I. Bray, Phys. Rev. Lett. **116**, 233201 (2016).
[5] L. H. Scarlett, D. V. Fursa, M. C. Zammit, I. Bray, Yu. Ralchenko, and K. D. Davie, At. Data Nucl. Data Tables **137**, 101361 (2021).
[6] L. H. Scarlett, D. V. Fursa, M. C. Zammit, I. Bray, and Yu. Ralchenko, At. Data Nucl. Data Tables **139**, 101403 (2021).
[7] H. Feshbach, Ann. Phys. (N.Y.) **5**, 357 (1958).
[8] J. Horáček, M. Cízek, K. Houfek, P. Kolorenč, and W. Domcke, Phys. Rev. A **73**, 022701 (2006).
[9] C. Mundel and W. Domcke, J. Phys. B **17**, 3593 (1984).
[10] J. Horáček, M. Čížek, K. Houfek, P. Kolorenč, and W. Domcke, Phys. Rev. A **70**, 052712 (2004).
[11] R. Celiberto, R. K. Janev, J. M. Wadehra, and J. Tennyson, Chem. Phys. **398**, 206 (2012).
[12] R. Celiberto, R. K. Janev, V. Laporta, J. Tennyson, and J. M. Wadehra, Phys. Rev. A **88**, 062701 (2013).
[13] V. Laporta, R. Agnello, G. Fubiani, I. Furno, C. Hill, D. Reiter, and F. Taccogna, Plasma Phys. Controlled Fusion **63**, 085006 (2021).
[14] M. C. Zammit, D. V. Fursa, J. S. Savage, and I. Bray, J. Phys. B **50**, 123001 (2017).
[15] A. S. Kadyrov and I. Bray, Phys. Rev. A **66**, 012710 (2002).
[16] J. S. Savage, Ph.D. thesis, Curtin University, 2018, http://hdl.handle.net/20.500.11937/77785.
[17] J. Brown and A. Carrington, *Rotational Spectroscopy of Diatomic Molecules* (Cambridge University Press, Cambridge, England, 2003), ISBN 0521530784.
[18] R. Celiberto, R. K. Janev, J. M. Wadehra, and A. Laricchiuta, Phys. Rev. A **77**, 012714 (2008).
[19] D. T. Stibbe and J. Tennyson, J. Phys. B **31**, 815 (1998).
[20] D. T. Stibbe and J. Tennyson, Phys. Rev. Lett. **79**, 4116 (1997).
[21] I. Bray and A. T. Stelbovics, Phys. Rev. A **46**, 6995 (1992).
[22] K. Bartschat, E. T. Hudson, M. P. Scott, P. G. Burke, and V. M. Burke, J. Phys. B **29**, 115 (1996).
[23] J. Comer and F. H. Read, J. Phys. B **4**, 368 (1971).
[24] U. Fano, Phys. Rev. **124**, 1866 (1961).
[25] Y. K. Yang, Y. Cheng, Y. Wu, Y. Z. Qu, J. G. Wang, and S. B. Zhang, New J. Phys. **22**, 123022 (2020).
[26] W. Kolos, K. Szalewicz, and H. J. Monkhorst, J. Chem. Phys. **84**, 3278 (1986).
[27] G. Staszewska and L. Wolniewicz, J. Mol. Spectrosc. **198**, 416 (1999).
[28] G. Staszewska and L. Wolniewicz, J. Mol. Spectrosc. **212**, 208 (2002).
[29] C. E. Kuyatt, J. A. Simpson, and S. R. Mielczarek, J. Chem. Phys. **44**, 437 (1966).